Dynamics of lasers with ultra-short optical feedback

O. Ushakov[a], S. Bauer[b], O. Brox[b], H-J. Wünsche[a,b], and F. Henneberger[a]

[a]Humboldt Universität zu Berlin, Institut für Physik, Newtonstr.15, 12489 Berlin, Germany
[b]Fraunhofer-Institut fr Nachrichtentechnik, Heinrich-Hertz-Institut
Einsteinufer 37, 10587 Berlin, Germany

ABSTRACT

The dynamical behavior of a single-mode laser subject to optical feedback is investigated in the limit, when the delay time is much shorter than the period of the relaxation oscillations. Use of an integrated DFB device allows us to control the feedback phase. The system shows a very rich manifold of the nonlinear phenomena. Among them two kinds of Hopf bifurcations associated with regular self-pulsations of different frequencies, fold and period doubling bifurcation.

Keywords: semiconductor laser, nonlinear dynamics, optical feedback, self-pulsations, mode-comutations

1. INTRODUCTION

The single-mode laser is a paradigm of self-organisation in dissipative systems.[1] At threshold it undergoes a transition from incoherent to coherent emission. One optical mode becomes undamped here in a Hopf bifurcation. Its contribution to the optical field is harmonically oscillating and dominates beyond threshold, giving rise to the high coherence. Distributed Feedback (DFB) semiconductor lasers come close to this ideal.[2] They exhibit continuous wave (CW) single mode emission up to high pump currents. Upon a perturbation the intensity returns back to the stationary CW value with a well damped relaxation oscillation (RO). Optical feedback can destabilise the CW state.[3] Phenomena like self-sustaining intensity pulsations, coherence collapse,[4] and others have been recently predicted and experimentally observed. Potential applications cover high-speed data transmission, cryptography,[5] etc. Optical feedback is usually achieved by combining the laser with an external mirror.

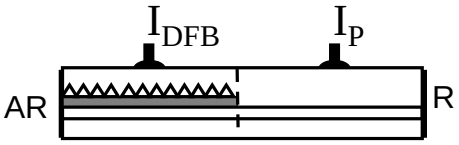

Figure 1. Scheme of the investigated DFB laser with integrated passive feedback section. The active zone (λ_g=1.55μm) is removed in the feedback section; the waveguide layer (λ_g =1.3μm) is common to both sections. $I_{\rm DFB}$: pump current DFB section, $I_{\rm P}$ pump current in feedback section.

The characteristic parameters are (i) the delay time τ through the round trip in the external cavity, (ii) the intensity fraction K^2 that re-enters the laser and (iii) the phase ϕ of the feedback field. The behavior in presence of feedback crucially depends on the number of modes that are of relevance in the compound device. This number grows when the feedback strength K increases. A second factor arises through the time-scales involved. Photon life-times in typical semiconductor lasers are $\tau_{\rm P} \approx$ 1-10 ps, while the period of the relaxation oscillations τ_R ranges between 0.1 and 1 ns. In the long-cavity limit, addressed in most previous studies, τ is much longer than τ_R. The solitary mode is hence transformed in a quasi-continuous spectrum of external cavity modes, even for modest K. The consequence is an irregular dynamical response with stochastic power dropouts. Studies on shorter cavities have yielded qualitatively different behavior.[3,15,16] Here, the feedback phase begins to influence the field-inversion dynamics in the laser. Regular intensity pulsations have been reported already in

Send correspondence to ushakov@physik.hu-berlin.de

early studies (see Ref. [3] and references therein). However the multimode nature of the used Fabry-Perot lasers mixes with feedback effects.[3] Using single mode lasers in a short feedback regime ($\tau/\tau_R \approx 0.3$ to 1), recently pulse packages have been observed that originate from a global trajectory along a limited number of modes in the phase-inversion space. The metamorphosis of this scenario with even shorter delay time was not subject to experiments yet. A certain exception are DFB lasers with active feedback used to generate self-pulsations of several ten GHz.[10] The dynamics of these devices is however modified by coupling the photons to two independent inversion ensembles.[11] Only the limit of feedback with zero delay is well known – the reflectivity from cleaved facets does not cause dynamic instabilities in DFB lasers.

In the present paper we consider structures, where laser and external cavity are monolithically integrated in a single device (Fig. 1). They enable to access the regime of very short cavities. Here, the length of both laser and feedback section is in the some 100-μm range resulting in $\tau/\tau_R \approx 0.01$. In this situation, two different pulsation phenomena are expected: mode-beating (MB) pulsations of mode–antimode pairs[7,8] and undamped RO[9,13] as well. Thus, the regime of pulse packages may be not the ultimate short-cavity limit with nontrivial dynamics.

The present paper summarizes the first experimental verification of these theoretical predictions. It is organised as follows: Device and experimental setup are described in Section 2. Sec. 3 reviews the observed dynamical scenarios. Phase tuning features are investigated in more detail in Sec. 4. A theoretical discussion of these experimental results in terms of optical modes and bifurcations is sketched in Sec. 5, followed by a detailed experimental verification of predicted bifurcations in in Sec. 6. We finish with some conlusions.

2. DEVICE AND SETUP

The investigated device is sketched in Fig. 1. It is based on InGaAsP-InP material system and the optical wave is guided by a ridge waveguide structure. It consists of two sections: a $L_{\mathrm{DFB}} = 220\mu$m long DFB laser is integrated with a passive feedback section of length $L_{\mathrm{P}} = 200\mu$m.

The active bulk $\lambda_{\mathrm{gap}} = 1.55\mu$m layer of the DFB laser is embedded in an asymmetric $\lambda_{\mathrm{gap}} = 1.3\mu$m InGaAsP optical waveguide which has an index coupled grating without phase shifts. A coupling coefficient $\kappa = 130\mathrm{cm}^{-1}$ was chosen in order to prevent mode switching between the two stop-band sides of the DFB laser. The short wavelength mode is supported by the resulting longitudinal hole burning. The facet of the DFB section is anti-reflection (AR) coated with a remaining power reflectivity 10^{-4}.

The feedback section behaves passive because the 1.55 μm layer is removed and the remaining layers do not directly couple to the emission of the laser. Its rear facet is cleaved, with a resulting power reflectivity $R \approx 0.3$. The feedback parameters are

$$\phi = -\frac{4\pi}{\lambda} n_{\mathrm{eff}} L_{\mathrm{P}}, \tag{1}$$

$$K = T_{\mathrm{AP}} \exp(-\alpha_{\mathrm{P}} L_{\mathrm{P}}) \sqrt{R}, \tag{2}$$

$$\tau = 2 L_{\mathrm{P}} v_g^{-1}. \tag{3}$$

The phase shift ϕ is proportional to the effective refractive index n_{eff} which in turn is affected by the carriers injected into this section. Therefore, the current I_{P} can be used for phase tuning at fixed laser parameters in contrast to previous studies exploiting laser current ([3] and references therein) or laser temperature[15,16] to these purposes. The measured phase tuning characteristics is shown in Fig. 2. More than 3 phase periods are accessible before the phase shift saturates beyond 80 mA. A secondary effect of I_{P} is a raising free-carrier absorption. It degrades the feedback strength K by roughly a factor 3 in the considered range of currents. Comparing with transmission spectra of non-biased isolated feedback sections cut from the same wafer, we estimated about 10 cm^{-1} background losses in the feedback cavity and a transmissivity T_{AP} of the active-passive interface close to unity. The corresponding feedback amplitudes range from $K \approx 0.3$ down to $K \approx 0.1$. The measured group index $c/v_g \approx 3.5$ is nearly independent of the phase current, yielding a constant delay $\tau \approx 5$ ps. The according round-trip frequency $\tau^{-1} \approx 200$ GHz is nearly two orders of magnitude larger than typical relaxation oscillation frequencies, the present device realises the limit of very short feedback cavities.

In order to detect and to characterise self-pulsations, the experimental setup of Fig. 3 is used. The two section laser is connected to the oscilloscope, the optical spectrometer and the electrical spectrum analyzer by a single

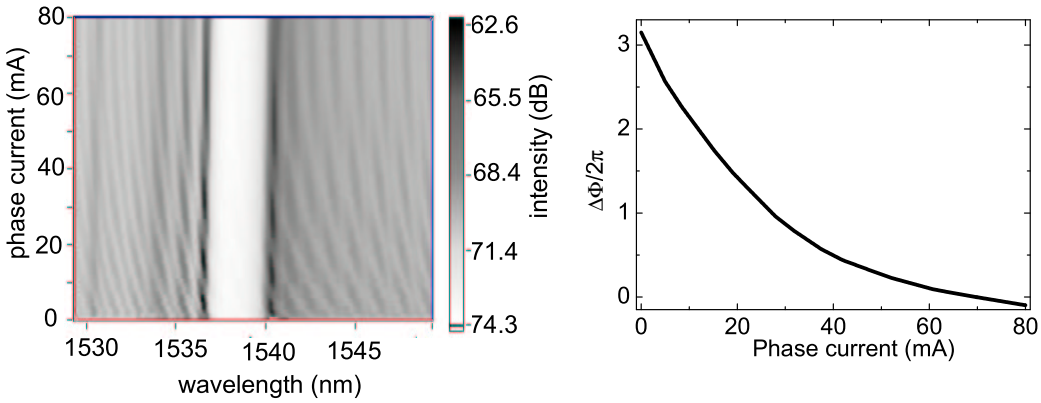

Figure 2. Phase tuning properties of the passive section. Left panel: movement of ASE ripples with the injection current of the feedback sectic ey scale. Right panel: Phase shift versus pl

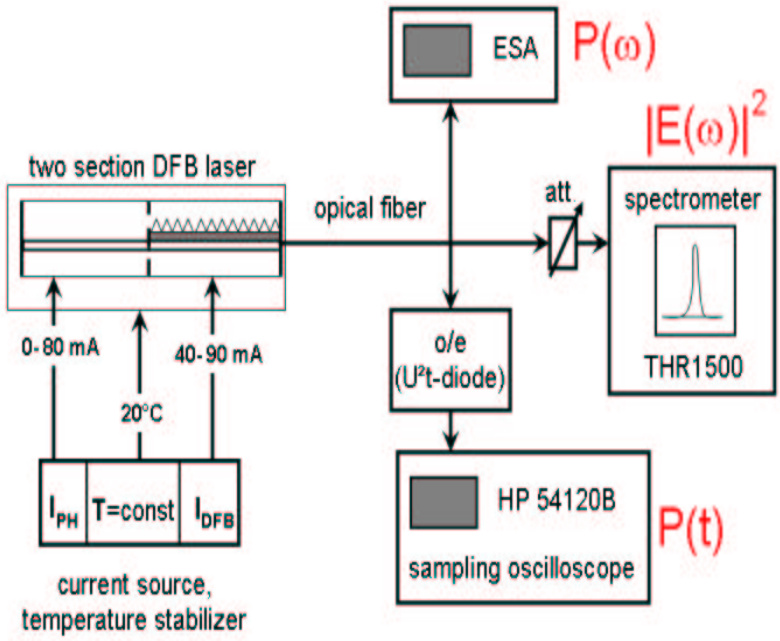

Figure 3. Experimental setup. The emission of the laser under investigation is analysed with a power spectrometer R&S FSP 9, a digital 50 GHz sampling oscilloscope (HP 54120B), and a Czerny-Turner spectrometer (0.015 nm resolution) with an infrared camera as detector.

mode optical fiber (SM Patchcord 9/125) from the DFB facet. The sampling oscilloscope (HP 54120B Digitize Oscilloscope) with an u2t photo diode is used to obtain time series. The bandwidth of the oscilloscope is 50 GHz. The optical spectra are measured by a Czerny-Turner spectrometer (THR 1500, with a grating 600g/mm) with an IR camera as detector. An attenuator between the laser and the spectrometer is to control the output intensity. Power spectra were measured by an electrical spectrum analyzer with a bandwidth of 40GHz (R&S FSP 9/40GHz) with an u2t photo diode. The time averaged mean power was measured by an optical power-meter (NOYES OPM 5), with averaging time 5s. The whole set of measurements are done at varying currents in the passive and active sections. Currents are controlled by the current source (PRO 8000). Both sections of the laser are kept at a constant temperature 20C^o, the stabilization of the temperature is about 0.05C^o.

3. REGIONS OF SELF-PULSATIONS

In order to find the theoretically predicted self-pulsations we map the two injection currents over a wide range. Depending on the point of operation, different types of RF and optical spectra are observed. Fig. 4 shows characteristic examples. A single line in the optical spectrum and a flat noise floor in the RF spectrum are

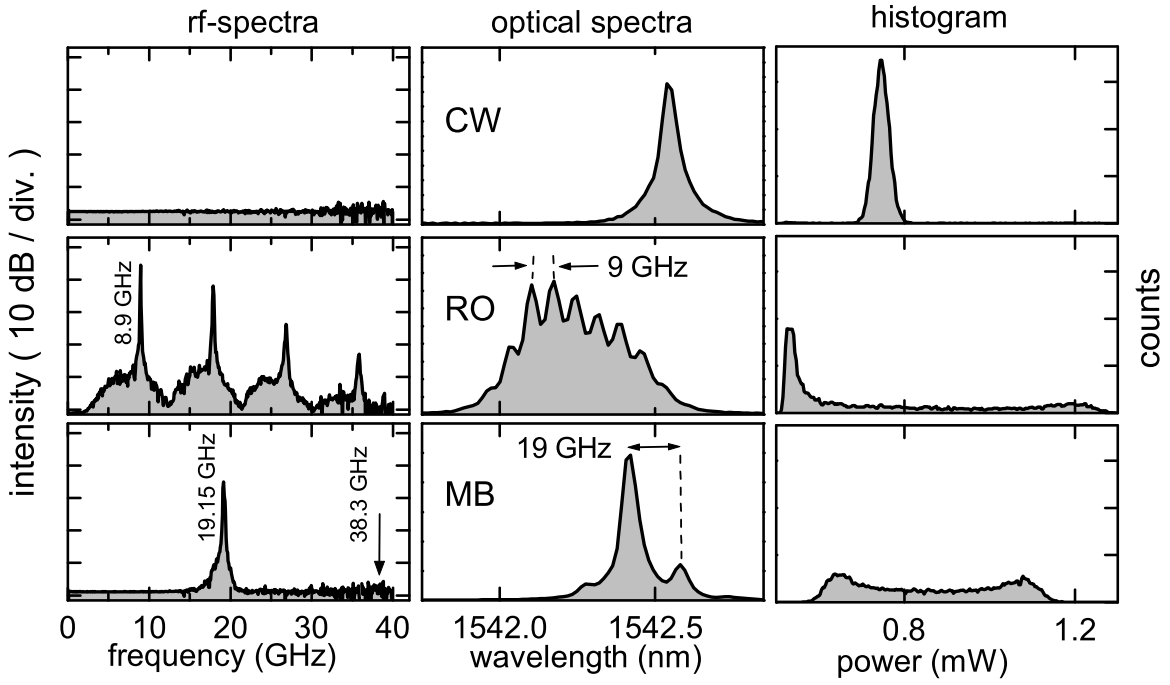

Figure 4. Characteristica of the most prominent types of laser emission. Left column: power spectra, middle column: optical spectra, right column: histograms. Upper row: CW emission (point CW of Fig. 5, $I_{\mathrm{DFB}} = 65$ mA, $I_{\mathrm{P}} = 45$ mA). Middle row: undamped RO pulsation (point RO of Fig. 5, $I_{\mathrm{DFB}} = 50$ mA, $I_{\mathrm{P}} = 28$ mA). Lower row: MB pulsation (point MB of Fig. 5, $I_{\mathrm{DFB}} = 70$ mA, $I_{\mathrm{P}} = 11$ mA).

attributes of CW emission. Sharp and strong RF peaks and a corresponding splitting of the optical emission line into several sublines are the fingerprints of self-pulsations. Fig. 5 shows the regions in the two-paremeter plane I_{DFB} – I_{P} where the major RF peak exceeds the noise floor by more than 5 dB.

Cycles of alternating SP and CW regimes appear in dependence on I_{P} due to the phase tuning property of this current. The injection level of the DFB section has only a small influence on the position of the SP islands. This influence is due to the change of the feedback phase with the emission wavelength. The SP islands of the different cycles are similar but not identical because I_{P} influences not only the phase but also the strength of feedback.

The frequencies of SP range from about 1 GHz up to 24 GHz. They increase sublinearly with I_{DFB} in the lower part of each SP island. This behaviour is a fingerprint of relaxation oscillations. We can conclude that those parts of the SP-islands, which continuously evolve from these low frequency parts are regions of undamped RO. Below we shall give more evidence for this conclusion. We shall also proof that the high-frequency parts of the islands are not RO pulsations, in particular the upper parts within the first two phase cycles.

The right column in Fig. 4 shows how frequent a given optical power is detected by the oscilloscope within a very long time. These histograms provide further statistical characteristics of the measured signals. The stationary state is represented by a single peak at the mean power. Its width is a measure for the noise induced intensity fluctuations. Regular pulsations are characterized by wide two-peak distributions. The peaks represent the mean minimum and maximum powers. Their heights measure how fast the intensity passes through the respective extrema. The RO histogram exhibits a high extinction ratio and a very distinct peak at the minimum

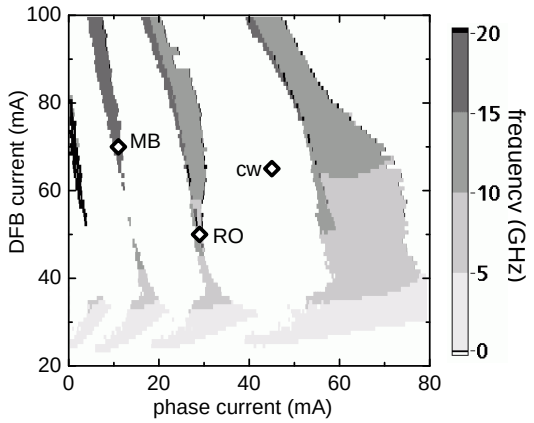

Figure 5. Self-pulsation regions in the plane of phase and DFB current. The grey levels code the frequency of the major peak in the RF spectrum. White: CW emission (major RF peak less then 5 dB above noise floor). Diamonds: points of operation presented in Fig. 4.

power. Thus, they are comparatively short pulses separated by relatively long valleys with minimum intensity. In contrast, the extinction of MB pulsations is smaller and the two similar peaks indicate a nearly sinusoidal behaviour.

4. PHASE TUNING

So far we have identified the regions and frequencies of self-pulsations. The phase current appeared as main parameter for the bifurcations from CW to SP. Now we give a deeper characterisation of the SP and of the bifurcations associated with the feedback phase. To these purposes we change the phase current in small 0.1 mA steps from 0 mA to 80 mA and reverse, keeping the DFB current at 50 mA. Mean intensity, modulation depth, and wavelength of the emission from the DFB facet are recorded in each point of operation. In Fig. 6, the data are plotted versus the phase parameter ϕ determined from I_{P} as described in Section 2.

Power and wavelength undergo cyclic variations with ϕ and exhibit distinct hysteresis effects due to the movement of external cavity modes across the fix DFB resonance. The power becomes maximum when a mode coincides with the resonance. With changing ϕ from here, this mode departs from optimum, the threshold increases and the power decreases until a jump to the next better mode appears. The regions of nonzero modulation depth in Fig. 6 c) are indications of self-pulsations. They appear for increasing phase (forward direction) in each period just before jumping to the next mode. Similar power and wavelength ondulations were observed when changing the injection current of a semiconductor laser subject to external optical feedback.[3]

The different periods are not completely equivalent because I_{P} changes not only the phase of the feedback but also its strength K from ≈ 0.3 down to ≈ 0.1 in the investigated current range (see Section 2). Obviously, hysteresis and pulsation effects are most sensitive to this effect. They qualitatively change from region ii to region iii.

In regions i and ii pulsations occur only with small amplitude in a small interval in forward direction and the frequencies are around 20 GHz as expected for MB pulsations. In the other two periods, the SP have distinctly smaller frequencies, higher amplitudes, and show less hysteresis.

5. THEORETICAL ANALYSIS

The above observations reveal a specific scenario that is analyzed now more closely. The longitudinal modes of the compound cavity, comprising DFB and feedback section, follow from the round-trip condition

$$q(\Omega, N)\exp(-i\Omega\tau) = K\exp(-i\phi), \tag{4}$$

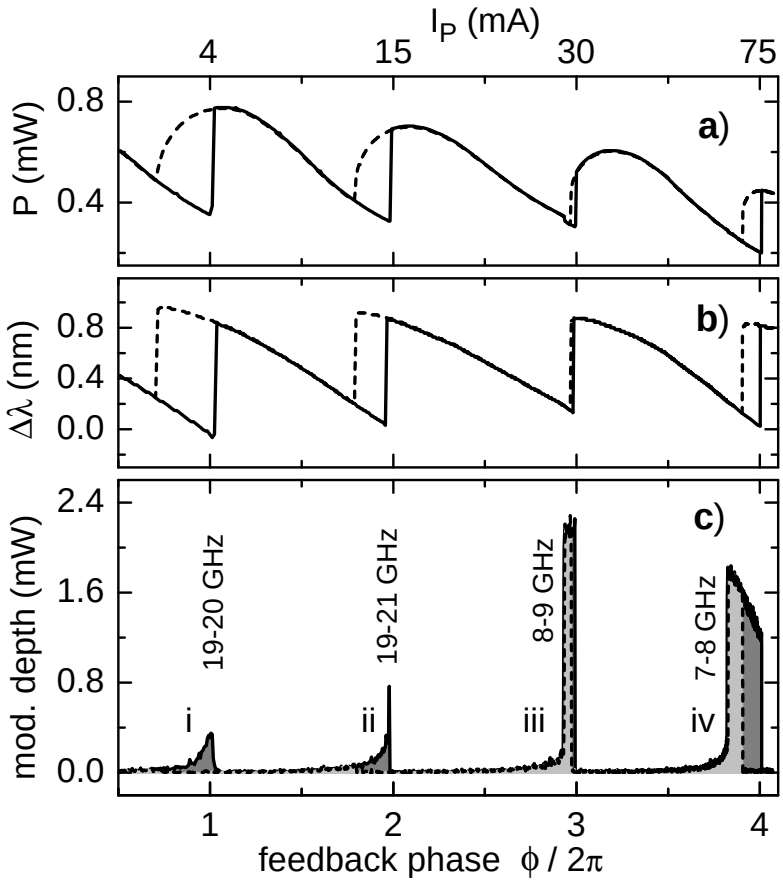

Figure 6. Control of the dynamics by phase tuning. Panel a): mean output power P. Panel b): shift $\Delta\lambda$ of the main peak in the optical spectrum Panel c): modulation depth M (difference between maximum and minimum on the sampling oscilloscope). Solid: increasing $I_{\rm P}$. Dotted: decreasing $I_{\rm P}$. The phase ϕ (bottom scale) is determined from the phase current (top scale) according to Fig. 2. The DFB current is kept at 50 mA.

where N is the average carrier density in the laser and Ω denotes the complex mode frequency, measured relative to the Bragg resonance at transparency. The DFB enters here by its inverse amplitude reflectivity[2]

$$q \quad = \quad \frac{i\gamma}{\kappa}\cot(\gamma L_{\rm DFB}) - \frac{\beta}{\kappa} \tag{5}$$

with $\gamma^2 = \beta^2 - \kappa^2$ and the propagation constant

$$\beta(\Omega, N) = \frac{1}{2}[(i+\alpha_H)g'(N-N_{tr}) - \alpha_0] + \frac{\Omega}{v_g}. \tag{6}$$

The parameters involved ($\kappa = 130\ \mathrm{cm}^{-1}$: coupling coefficient of index grating , $\alpha_H = -5$: linewidth enhancement factor, $\alpha_0 = 25\ \mathrm{cm}^{-1}$: background absorption, $g' = 10^{-20}\ \mathrm{m}^2$: differential gain, including the transverse confinement factor, $N_{\rm tr} = 10^{24}\ \mathrm{m}^{-3}$: carrier density at transparency level) have been deduced from independent measurements.

The solutions of the complex valued Eq. (4) are quite complex surfaces in the threedimensional space spanned by ReΩ, ImΩ, and N. Fig. 7 depicts these solutions by curves of constant K and constant ϕ in two different plane cuts through this space. The modes of the solitary laser ($K = 0$) are represented by vertices, where the equi-phase lines move together. The left panels show the so-called external cavity modes. They belong to a fixed N, here the threshold density of the solitary laser. Obviously, the very short delay of our device has already a

considerable impact on the mode structure. Without delay, curves of constant feedback strength $\mid q(\Omega, N) \mid = K$ are orbits around the mode of the solitary laser. Their extension is an increasing function of K. With delay, the factor $\exp(i\Omega\tau)$ in Eq. 4 gives rise to additional modes. At small $K = 0.1$, these new external cavity modes are highly damped and located on a separate line well above the orbit of the central laser mode. At the higher $K = 0.3$, this line has moved down and it merged with the central orbit forming a deep valley.

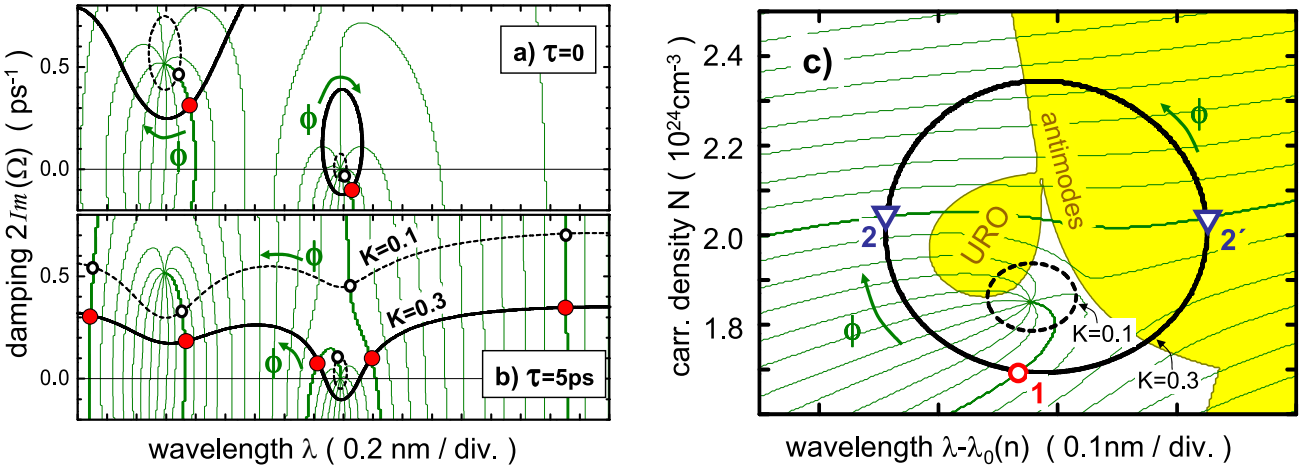

Figure 7. Modes calculated from Eqs. (4 to 6). Curves of constant feedback ($K = 0.1$ dashed, $K = 0.3$ solid) and curves of constant phase (thin grey, 10 lines per phase period) are drawn in all panels. Panels a) and b): External cavity modes in the damping-wavelength plane, carriers fixed to the threshold density of the solitary DFB laser. Panel c): Compound cavity modes in the wavelength-density plane Im(Ω)=0. The carrier-induced shift $\lambda_0(N)$ is subtracted here for clarity. Grey area: regions of instability.

Fig. 7c shows the central part of the same scenario in terms of modes at threshold, often called compound cavity modes. Standard single-mode stability analysis[6] of these modes yields two types of instabilities: saddles in the region labelled 'anti-modes' and undamped relaxation oscillations in the small island denoted by 'URO'. The grey borders of these islands represent saddle-node and Hopf bifurcations, respectively. The orbit $K = 0.1$ touches the 'URO' island but not the more extended orbit $K = 0.3$. This island topology explains, why RO pulsations are only found in higher phase periods of I_P (see Fig. 5), as K is sufficiently reduced here. It is also consistent with the observation of similar Hopf bifurcations for longer cavities.[16] Undamped relaxation oscillations are hence a common feature of short and ultra-short cavities with weak feedback.

While the form of the orbit in the right panel is independent on τ, the delay controls the number of modes enclosed. For small K, it holds $\exp(i\Omega\tau) \approx 1$ along the orbit. Only one mode exists that rotates with ϕ clockwise around the orbit. However, variation of $\Omega\tau$ along extended orbits is associated with a change of ϕ by more than one period, enabling thus several modes. It is this interrelation between feedback delay and strength that gives rise to new dynamics, even though $\tau/\tau_R \ll 1$. The variation of ϕ is not monotonous along the orbit. The equi-phase lines are tangential with the orbit, where it enters the anti-mode region. Pairs of modes appear or disappear here in saddle-node bifurcations. With increasing ϕ, the stable modes move up on the left part of the loop, while the unstable anti-modes do so on the right-hand side.

At a particular phase, mode and antimode arrive at comparable threshold densities (triangles). Here, both modes accommodate to each other at a common density and MB pulsations emerge in a Hopf bifurcation.[7,9,13] This scenario is reminiscent of the bifurcation bridges predicted for long delay times.[8] The peculiar feature of the ultra-short cavity regime is the existence of only one anti-mode, yielding regular dynamics, whereas the pulse-package scenario[16] involves multiple anti-modes. The device output is therefore qualitatively different. Pulse packages are pulse sequences with a repetition rate exactly given by the external cavity frequency $1/\tau$, amplitude-modulated with a frequency below $1/\tau_R$. At variance, the MB pulsations are not modulated and their frequency is by about one order of magnitude smaller than $1/\tau$, due to pulling of the side-mode by the DFB

resonance. The transition between both regimes is an interesting subject of future research. We note finally that the instability above state 2 is also the source of the hysteresis observed experimentally. For decreasing ϕ, state 1 moves to longer wavelengths and, in contrast to forward phase, reaches the saddle-node bifurcation. Here, the laser switches to the only stable state of same ϕ on the left part of the orbit, about three phase grids below state 2.

6. BIFURCATIONS

So far we have shown how two different types of SP can be generated by properly choosing the phase current. Theory predicts both types of SP to be born in a Hopf bifurcation,[8,9,13] which is the classical scenario of temporal self-organisation. Now we search for experimental evidence for this prediction.

Mathematically a Hopf bifurcation is characterised by a pair of complex conjugated eigenvalues of the dynamical matrix moving across the imaginary axis. What does it mean from physical point of view? Among many vibrational modes there is one oscillator whose damping approaches zero. In order to detect this process experimentally, we can profit from the noise in our real system, which is omnipresent e.g. due to spontaneous emission. Noise drives all possible oscillations. If the damping of one oscillator approaches zero, its oscillation amplitude increases. An increasing and narrowing line should appear in the power spectrum as a precursor of the Hopf bifurcation, whose position and width are a direct measure for the relevant complex eigenvalues.

6.1. subcritical Hopf bifurcation

First we apply this concept to the SP region iii of Fig. 6. The modulation depth re-plotted in a zoomed scale is going to exceed the noise level when approaching the pulsation region from left. This amplitude increase is already the fingerprint of an oscillator getting undamped. At the same time, a well resolvable line in the rf spectra appears (see of Fig. 8). The distinct decay of its width is evidence of a Hopf bifurcation at this boundary of the self-pulsation region.

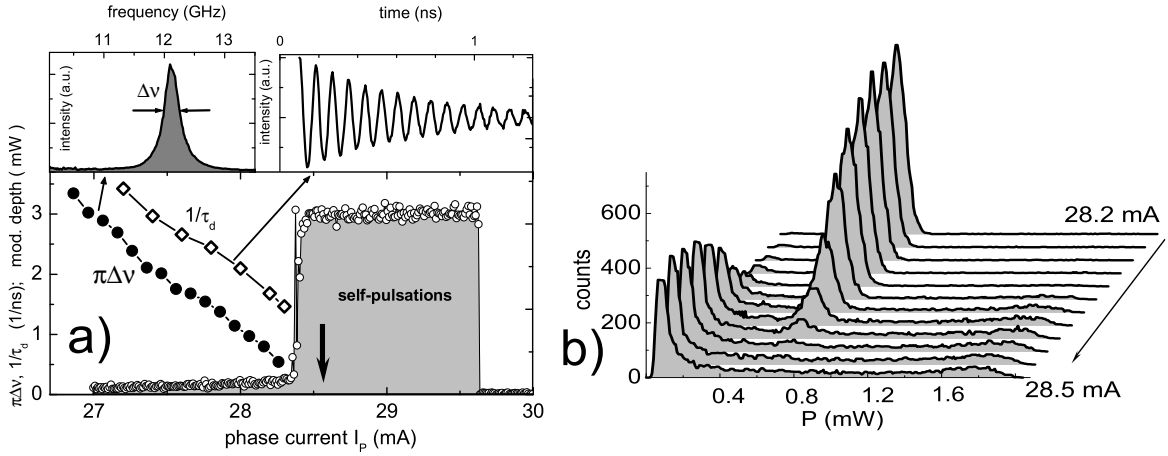

Figure 8. a) Characteristics of the Hopf-bifurcation of relaxation-oscillation self-pulsations. DFB current at 50 mA. Small circles: modulation depth. Full circles: half-width $\pi\Delta\nu$ of the resonance line in the rf spectrum. Open circles: damping rate τ_d^{-1} of relaxation oscillations. Both linewidth and decay rate approach to zero. The horizontal offset of the decay rates is possibly due to a change of the point of operation caused by the external excitation. b) Set of histograms with a change of the phase current.

In order to evaluate the physical nature of the undamped oscillator, the laser was excited by an external pulse and the decaying response was measured (see inset of Fig. 8). The decay rates fall with the same slope as the rf linewidths. Thus, the oscillations undergoing the Hopf-bifurcation are relaxation oscillations. The small deviation between measured resonance widths and decay rates is possibly due to a small impact of the external excitation on the feedback phase.

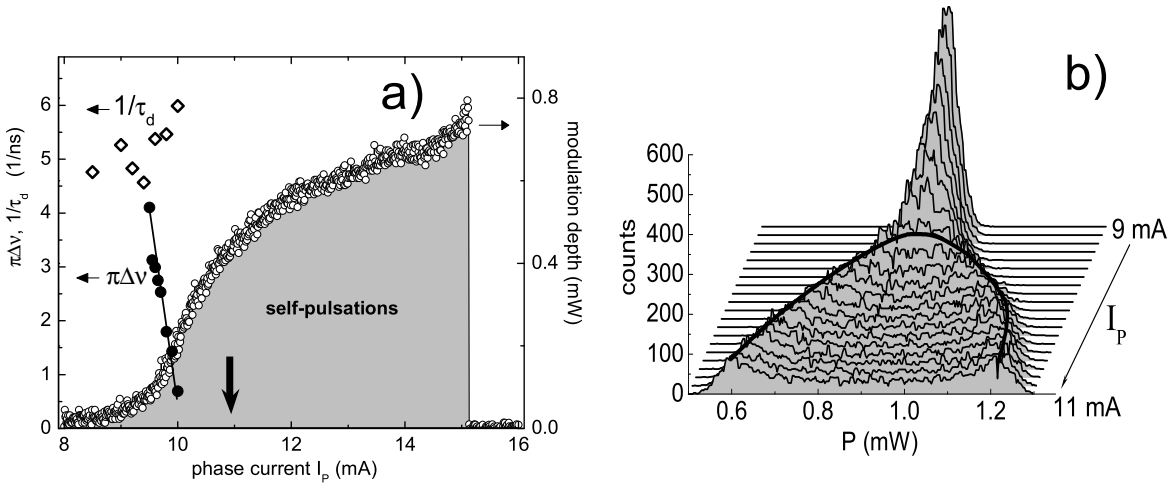

Figure 9. a) Characteristics of the Hopf-bifurcation of mode-beating self-pulsations. DFB current at 70 mA Small circles: modulation depth. Full circles: half-width $\pi\Delta\nu$ of the resonance line in the rf spectrum. Open circles: damping rate τ_d^{-1} of relaxation oscillations. b) Set of histograms with a change of phase current.

The frequency of the decaying oscillations is 12 GHz in agreement with the rf-peak positions, distinctly above the RO resonance of comparable DFB lasers without feedback. This finding is a typical effect of undamping by dispersive Q-switching which is accompanied by an increase of the effective differential gain.

The modulation depth suddenly blows up when crossing the bifurcation accompanied by a slowing down of the oscillations from 12 GHz to 9 GHz. However, no hysteresis is observable within the experimental resolution indicating a regime close to the transition from a subcritical Hopf to a supercritical Hopf.

The evolution of pulsations can also be observed in the histograms (Fig. 8b). The stationary state at 28.2 mA is represented by a single peak with about 0.8 mW mean power. At 28.5 mA, the histogram shows the typical features of RO pulsations. However, this transition is not sudden as might be concluded from panel a). In a finite intermediate range, the RO-peaks appear smoothly in the same manner as the single cw-peak drops down. We attribute this phenomenon to noise induced transitions between the two stable attractors close to the subcritical Hopf bifurcation. Obviously, the transitions from cw to RO and back appear with comparable probabilities within this range. Thus, the investigated point of operation is very close to a codimension two bifurcation, where the Hopf changes its character from subcritical to supercritical.

6.2. supercritical Hopf bifurcation

The same technique is applied now to the mode-beating pulsations on a horizontal cut crossing point MB in Fig.a) 5. The spectra of the SP along the cut are similar to that in point MB (Fig. 4). They indicate nearly sinusoidal mode-beating pulsations with frequencies around 20 GHz. The left boundary of the pulsation region depicted in Fig. 9 is not sharp, the modulation depth raises smoothly here. However, the mode-beating line in the power spectrum emerges from a precursor whose width falls rapidly when approaching the pulsation region. Thus, the mode-beating pulsations are also born in a Hopf bifurcation as predicted theoretically.[8] The measured decay rates of relaxation oscillations keep high along this bifurcation. Thus, the oscillator undergoing the Hopf bifurcation is not connected with the relaxation oscillations.

The evolution of the histograms in Fig. 9b exibits similar tendencies as previously observed in the case of the subcritical Hopf bifurcation. The height of the main peak decreases and its width increases with the increase of the current. However, the two peaks of the pulsating state appear now in a smooth transitions which clearly resembles the features of a supercritical Hopf bifurcation.

7. CONCLUSION

A single-mode DFB laser with an biased passive feedback cavity has been investigated experimentally. Although the 5 ps feedback delay is shorter by two orders of magnitude compared to the period of relaxation oscillations, it is crucial for the dynamics of the device. Two different types of self-sustaining intensity-pulsations are detected depending on strength and phase of the feedback which are controlled by the bias to the passive section. One type of pulsations is emerging in a Hopf-bifurcation from relaxation oscillations. These oscillations become undamped due to dispersive self-Q switching. The second type of pulsations is a mode-antimode beating pulsation. It is also born in a Hopf bifurcation. These findings give first experimental evidence for recent theoretical predictions.[8,9] A supplementary mode and stability analysis agrees well with measurements and it is used to discuss the relations to intermediate-delay[16] as well as zero-delay regimes.

REFERENCES

1. H. Haken, *Laser Theory* (Springer-Verlag, 1986).
2. John E. Carroll, J.E.A. Whiteaway, R.G.S. Plumb and D. Plumb, *Distributed Feedback Semiconductor Lasers* (IEE Publishing, 1998).
3. R. Lang and K. Kobayshi, *IEEE J. of Quant. El.*, QE-**16**, 347-355 (1980).
4. I. Fischer, T. Heil, M. Münkel, and W. Elsässer, in *Proceedings of SPIE* , vol. 3283, pp. 571–579 (1998).
5. J. Ohtsubo, *IEEE J. of Quant. El.*, QE-**38**, 1141 (2002).
6. Vasile Z. Tronciu, H-J. Wünsche, J. Sieber, K. Schneider and F. Henneberger, Opt. Comm. **182**, 221 (2000).
7. A. Tager and K. Petermann, *IEEE J. of Quant. El.*, QE-**30**, 1553-1561 (1994).
8. T. Erneux *et al.*, Opt. Comm. **183**, pp. 467-477 (2000)
9. J. Sieber, *SIAM J. of Appl. Dyn. Sys.* vol. **1**, 248 (2002).
10. S. Bauer et al. *Electron. Lett.*, vol. **38**, pp. 334-335 (2002)
11. S. Bauer et al., Phys. Rev. E **69**, 016206 (2004)
12. H-J. Wünsche, O. Brox, M. Radziunas, F. Henneberger, *Phys. Rev. Lett.* **88**, 023901 (2002).
13. M. Wolfrum and D. Turaev, *Opt. Comm.*, vol. **212**, pp. 127-138, 2002.
14. B. Sartorius, *et al.*, *IEEE Photonics Technol. Lett.*, vol. **7**, 1261 (1995)
15. T. Heil, I. Fischer, W. Elsäer, and A. Gavrielides, *Phys. Rev. Lett.*, vol. **87**, 243901 (2001)
16. T. Heil, I. Fischer, and W. Elsäßer, B. Krauskopf and K. Green, A. Gavrielides, Phys. Rew. E **67**, 066214, 2003.